The Journal of Immunology

DUSP3 Genetic Deletion Confers M2-like Macrophage–Dependent Tolerance to Septic Shock

Pratibha Singh, Lien Dejager, Mathieu Amand, Emilie Theatre, Maud Vandereyken, Tinatin Zurashvili, Maneesh Singh, Matthias Mack, Steven Timmermans, Lucia Musumeci, Emmanuel Dejardin, Tomas Mustelin, Jo A. Van Ginderachter, Michel Moutschen, Cécile Oury, Claude Libert and Souad Rahmouni

J Immunol published online 15 April 2015
http://www.jimmunol.org/content/early/2015/04/15/jimmunol.1402431

The Journal of Immunology is published twice each month by The American Association of Immunologists, Inc., 9650 Rockville Pike, Bethesda, MD 20814-3994.

Print ISSN: 0022-1767 Online ISSN: 1550-6606.

Published April 15, 2015, doi:10.4049/jimmunol.1402431

DUSP3 Genetic Deletion Confers M2-like Macrophage–Dependent Tolerance to Septic Shock

Pratibha Singh,*[,1] Lien Dejager,[†,‡,1] Mathieu Amand,*[,1] Emilie Theatre,[§] Maud Vandereyken,* Tinatin Zurashvili,* Maneesh Singh,* Matthias Mack,[¶] Steven Timmermans,[†,‡] Lucia Musumeci,* Emmanuel Dejardin,[‖] Tomas Mustelin,[#,] Jo A. Van Ginderachter,[††,‡‡] Michel Moutschen,* Cécile Oury,[§§] Claude Libert,[†,‡,2] and Souad Rahmouni*[,2]**

DUSP3 is a small dual-specificity protein phosphatase with an unknown physiological function. We report that DUSP3 is strongly expressed in human and mouse monocytes and macrophages, and that its deficiency in mice promotes tolerance to LPS-induced endotoxin shock and to polymicrobial septic shock after cecal ligation and puncture. By using adoptive transfer experiments, we demonstrate that resistance to endotoxin is macrophage dependent and transferable, and that this protection is associated with a striking increase of M2-like macrophages in DUSP3$^{-/-}$ mice in both the LPS and cecal ligation and puncture models. We show that the altered response of DUSP3$^{-/-}$ mice to sepsis is reflected in decreased TNF production and impaired ERK1/2 activation. Our results demonstrate that DUSP3 plays a key and nonredundant role as a regulator of innate immune responses by mechanisms involving the control of ERK1/2 activation, TNF secretion, and macrophage polarization. ***The Journal of Immunology*****, 2015, 194: 000–000.**

Sepsis and septic shock are complex clinical syndromes that cover a spectrum of pathophysiological conditions resulting from the response to infection (1). Sepsis develops when the inflammatory immune response to infection is uncontrollably amplified (2). The inflammation is usually initiated by recognition of bacterial components such as bacterial LPS. This leads to the activation of TLR4 signaling cascades and results in excessive release of cytokines, chemokines, and NO, which can initiate widespread tissue injury leading to organ dysfunction and eventually to death (3).

NF-κB and the MAPKs signaling pathways are the major pathways activated after TLR4 stimulation (4). This leads to the expression of target genes encoding various inflammatory cytokines, such as TNF and IL-6 (4, 5). MAPKs activation is regulated by phosphorylation by MAPKinase kinase kinases (6). MAPKs are inactivated by different protein phosphatases, including the dual-specificity protein phosphatases (DSPs), to terminate MAPK-induced signaling. The human genome contains 30 protein-encoding *DSP/DUSP* genes. Eleven of these DSPs, called MAPK phosphatases (MKPs), contain a MAPK binding domain. The other 19 are atypical DSPs (A-DSPs) that do not contain this domain (7, 8). MAPKs are mainly regulated by MKPs. Analysis of mice lacking a specific MKP-coding gene has shown that MKPs are not functionally redundant and that they have important effects on immune responses (9–11). In contrast with the MKPs, the physiological functions of A-DSPs are largely unknown.

DUSP3, also called *Vaccinia*-H1–related phosphatase (VHR), is a 21-kDa A-DSP encoded by *DUSP3* in humans (*Dusp3* in mice). DUSP3 has been reported to dephosphorylate the MAPKs ERK and JNK, but not p38 (12–14). We previously reported that, unlike MKPs, DUSP3 expression is not induced in response to MAPKs activation but is regulated during cell-cycle progression (15, 16). We, and others, have also reported that DUSP3 expression levels are altered in several human cancers (17–19). We recently generated DUSP3-knockout (DUSP3$^{-/-}$) mice and found that they were healthy, fertile, and showed no spontaneous phenotypic abnormality. However, DUSP3 deficiency prevents neoangiogenesis and basic fibroblast growth factor–induced microvessel outgrowth (20). In this study, using DUSP3$^{-/-}$ mice, we identified DUSP3 as a key and nonredundant regulator of the innate immune response to lethal inflammatory shock induced by endotoxin or poly-

*Laboratory of Immunology and Infectious Diseases, GIGA-Signal Transduction Unit, University of Liège, B-4000 Liège, Belgium; [†]Inflammation Research Center, VIB, B-9052 Ghent, Belgium; [‡]Department of Biomedical Molecular Biology, Ghent University, B-9000 Ghent, Belgium; [§]Laboratory of Animal Genomics, GIGA-Genetics Unit, University of Liège, B-4000 Liège, Belgium; [¶]Department of Internal Medicine II, University Hospital Regensburg, 93042 Regensburg, Germany; [‖]Laboratory of Molecular Immunology and Signal Transduction, GIGA-Signal Transduction Unit, University of Liège, B-4000 Liège, Belgium; [#]Signal Transduction Program, Sanford-Burnham Institute, La Jolla, CA 92037; **MedImmune, Gaithersburg, MD 20878; [††]Laboratory of Cellular and Molecular Immunology, Vrije Universiteit Brussel, B-1050 Brussels, Belgium; [‡‡]Myeloid Cell Immunology Laboratory, VIB, B-1050 Brussels, Belgium; and [§§]Laboratory of Thrombosis and Hemostasis, GIGA-Cardiovascular Sciences Unit, University of Liège, B-4000 Liège, Belgium

[1]P.S., L.D., and M.A. contributed equally to this work.

[2]C.L. and S.R. contributed equally to this work.

ORCID: 0000-0003-0956-0242 (S.R.).

Received for publication September 24, 2014. Accepted for publication March 9, 2015.

This work was supported by the Fonds Léon Fredericq, the Fonds de la Recherche Scientifique-Fonds National de la Recherche Scientifique, the Fonds Spéciaux Pour la Recherche de l'Université de Liège (to S.R.), the Fonds Wetenschappelijk Onderzoek (to C.L. and L.D.), the Interuniversity Attraction Poles (to C.L.), and National Institutes of Science Grant 5R01AI035603 (to T.M.). P.S., M.A., and M.V. are Fonds National de la Recherche Scientifique-Télévie Ph.D. fellows.

The sequences presented in this article have been submitted to National Center for Biotechnology Information Gene Expression Omnibus under accession number GSE66782.

Address correspondence and reprint requests to Dr. Souad Rahmouni, Laboratory of Immunology and Infectious Diseases, GIGA-Signal Transduction Unit, University of Liège, GIGA B34, Avenue de l'Hôpital 1, B-4000 Liège, Belgium. E-mail address: srahmouni@ulg.ac.be

Abbreviations used in this article: A-DSP, atypical DSP; BM, bone marrow; CBA, cytokine bead array; CLP, cecal ligation and puncture; DSP, dual-specificity protein phosphatase; DUSP3$^{-/-}$, DUSP3-knockout; β2M, β2-microglobulin; MKP, MAPK phosphatase; PM, peritoneal macrophage; VHR, *Vaccinia*-H1–related phosphatase.

microbial infection, and showed that it acts by a mechanism involving M2-like macrophages. Moreover, we report that DUSP3 is required for the production of TNF and, therefore, contributes to inflammatory responses.

Materials and Methods

Human RNA sampling

RNA was prepared from sorted human blood cells obtained from 256 healthy volunteers. Donors were informed about the objectives of the study and signed an informed consent. The ethical committee review board of the University Hospital of Liège approved the study. Venous blood (5 ml) was collected on EDTA. $CD19^+$ B lymphocytes, $CD4^+$ and $CD8^+$ T lymphocytes, $CD14^+$ monocytes, and $CD15^+$ granulocytes were positively selected from PBMCs using MACS separation columns (Miltenyi Biotec). Total RNA was extracted from freshly purified cell populations using AllPrep DNA/RNA Micro Kit (Qiagen) and stored at −80˚C until use. RNA was quantified by absorbance measurement, and 200 ng RNA was used in reverse transcription with oligo-dT primers (Superscript III RT; Invitrogen), before biotin labeling and amplification using the TargetAmp Nano-g Biotin-aRNA Labeling Kit for the Illumina System (Epicentre). Biotin-labeled aRNA were purified using the RNeasy MinElute Cleanup Kit (Qiagen) and 400 ng was hybridized on Human HT-12 v4 arrays (Illumina) following the recommendations of the manufacturer. Arrays were scanned on an iScan microarray scanner (Illumina). Internal quality controls of the arrays were analyzed. Cell-specific expression markers were analyzed in all samples to identify potential sample inversion or contamination. The raw fluorescence intensities for the probes corresponding to DSPs were corrected for the fluorescence background signal for each sample on the array by subtracting the fluorescence intensity of the negative control probes on the array. The data were then normalized by dividing the intensity for each probe in each sample by the mean fluorescence intensity of seven housekeeping genes in the same sample.

Mice

$DUSP3^{-/-}$ mice were generated as previously reported (20). These mice were backcrossed with C57BL/6 mice (Charles River) for 11 generations under specific pathogen-free conditions at the animal facility of Liège University. Heterozygotes breeding pairs were used to generate homozygote $DUSP3^{-/-}$ and paired $DUSP3^{+/+}$ littermate controls colonies used in the experiments. Mice were genotyped using DNA extracted from tail samples as previously described (20). Age-matched $DUSP3^{+/+}$ and $DUSP3^{-/-}$ female mice were used in all the experiments. C57BL/6-CD45.1 mice (Charles River) were used as recipient mice in the bone marrow (BM) and monocyte adoptive transfer experiments. Mice were kept in a specific pathogen-free animal facility and received food and water ad libitum.

All mouse experiments and procedures were approved by the animal ethics committees of the Universities of Ghent and Liège and were carried out according to their guidelines.

Abs and reagents

The following materials were from BD Biosciences: purified anti-CD16/CD32 (FcγIII/IIR) (2.4G2), PerCP–Cy5.5–anti-CD11b/Mac-1 (M1/70), PE–anti-CD14 (rmC5-3), allophycocyanin–anti-F4/80 (BM8), V450–anti-CD45.1 (A20), PE–Cy7–anti-CD45.2 (104), allophycocyanin–Cy7–anti-Ly6G (1A8), V500–anti–I-A/I-E (MHCII) (M5/114.15.2), and allophycocyanin–anti-CD11c (HL3). PE–anti-TLR4/MD2 (MTS510) was from eBioscience. FITC–anti-Ly6B (7/4), Alexa 647–anti-Ly6B (7/4) and Alexa 488–anti-Ly6G (ER-MP20) were from AbD Serotec. Anti-VHR (DUSP3) Ab (used for human samples 4752), anti–phospho-ERK1/2 (Thr^{202}/Tyr^{204}), anti-ERK1/2, anti–phospho-p38 (Thr^{180}/Tyr^{182}), anti-p38, anti–phospho-MEK1/2 ($Ser^{217/221}$) (42G9), anti-MEK1/2, and anti-Iκβα were from Cell Signaling. Anti-VHR (DUSP3) Ab used for mouse samples was from Santa Cruz (sc8889). Anti-GAPDH Ab was from Sigma. HRP-conjugated anti-goat, anti-mouse, and anti-rabbit Abs, used as secondary Abs, were from Amersham Biosciences (Glattbrugg, Switzerland). LPS from *Escherichia coli* serotype O111:B4 was from Sigma and was diluted in pyrogen-free PBS.

Cecal ligation and puncture and in vivo challenge with LPS

Cecal ligation and puncture (CLP) was performed as previously described (21). For LPS challenge, mice were i.p. injected with LPS (6 mg/kg). Body temperature was monitored using a rectal thermometer at various times after LPS injection and after CLP. Death of mice was recorded and the data were analyzed for statistical significance of differences between groups.

Mice irradiation, BM transplantation, and monocyte transfer

Donor mice 7–8 wk old were killed by cervical dislocation. Tibia and fibula were collected and BMs were flushed with PBS. BM cells (10×10^6) were immediately transplanted to recipient mice aged 7–8 wk that had been lethally irradiated (866.3 cGy). After 3–4 wk, transplantation efficiency was evaluated on the basis of the ratio of CD45.2 (donor) to CD45.1 (recipient) cells in the blood of transplanted mice.

For monocyte transplantation, monocytes were negatively selected from BM cell suspensions using an EasySep monocyte selection kit following the instructions of the manufacturer (STEMCELL). Monocytes (1.5×10^6) were injected i.v. into mice 24 h before LPS injection. Survival and body temperature were monitored for 8 d. Percentage and phenotype of transferred monocytes were evaluated by flow cytometry on peritoneal lavages of recipient mice using anti-CD45.1, anti-CD45.2, anti-CD11b, anti-F4/80, and anti-Ly6B Abs.

Isolation of peritoneal macrophages

Resident peritoneal macrophages (PMs) were selected by adherence to tissue culture plastic dishes in culture conditions at a cell density of 1×10^6 cells /ml in complete RPMI 1640 medium. After 2 h, cells were gently rinsed twice with FBS/RPMI 1640 and used for experiments.

Animal blood sampling and plasma preparation

Peripheral blood was drawn in EDTA-coated tubes (BD Microtainer K2E tubes; BD Biosciences) by puncturing the submandibular vein of the mouse with a sterile Golden rod animal lancet with a point length of 5 mm (Bioseb). Centrifugation was performed at 2000 rpm for 15 min at room temperature. Plasma samples were separated in sterile Eppendorf tubes, aliquoted in small volumes, and stored at −80˚C until used.

NO and urea levels

NO and urea levels were measured in plasma samples using Nitrate/Nitrite Fluorimetric Assay Kit (Cayman) and QuantiChrom Urea Assay Kit (DIUR-500; BioAssay Systems) according to the manufacturers' protocols.

Cytokine bead array

Levels of TNF and IL-6 in mouse plasma samples, peritoneal lavages, and supernatants of cultured macrophages were measured using a BD Biosciences cytokine bead array (CBA) mouse inflammation kit according to the manufacturer's protocol. Data were acquired using FACSCanto II, and results were analyzed using FCAP Array software (BD Biosciences).

Bacterial load in peritoneal cavity and blood

Mice were killed at various times after CLP, and peritoneal lavage was collected, diluted, and plated on brain heart infusion agar plates (BD Biosciences). Blood from the same animals was diluted in PBS at 1:2 before plating. Plates were incubated at 37˚C overnight and colonies were counted.

Flow cytometry and phenotyping

For surface cell staining, $2–5 \times 10^5$ cells were incubated for 15–20 min with anti-CD16/CD32 (FcγIII/IIR) before labeling for 30 min with specific Abs. All staining was done on ice in PBS supplemented with 1% BSA followed by one washing in cold PBS. Cells were next analyzed on FACSCanto II (Becton Dickson) using FlowJo (Tree Star).

Protein extraction, Western blot analysis, and JNK kinase assay

Protein extraction, Western blot analysis, and JNK kinase assay were performed as previously reported (20).

RNA purification, reverse transcription, and real-time PCR

RNA was extracted from PMs using a Roche kit (Roche) according to the manufacturer's instructions. cDNA was synthesized using Expand reverse transcriptase according to the recommendations of the manufacturer. cDNA was amplified using Sybr Green PCR Master Mix (Roche) and 0.3 μM specific primers for TNF-α, IL-6, and β2-microglobulin (β2M).

All quantitative PCR were performed on a LightCycler System for Real-Time PCR (Roche). The ratio between the expression level of the gene of interest and β2M in the sample was defined as the normalization factor. Relative mRNA quantities for TNF-α and IL-6 were determined by dividing the values interpolated from the standard curve by the normalization factor.

The sequences of the primers (Eurogentec, Seraing, Belgium) are as follows: TNF: forward (FW), 5′-CCAGTGTGGGAAGCTGTCTT-3′, re-

verse (RV), 5′-AAGCAAAAGAGGAGGCAACA-3′; IL-6: FW, 5′-ATGGATGCTACCAAACTGGAT-3′, RV, 5′-TGAAGGACTCTGGCTTTGTCT-3′; inducible NO synthase: FW, 5′-GCTTCTGGTCGATGTCATGAG-3′, RV, 5′-TCCACCAGGAGATGTTGAAC-3′; Arg1: FW, 5′-CAGAAGAATGGAAGAGTCAG-3′, RV, 5′-CAGATATGCAGGGAGTCACC-3′; Ym1: FW, 5′-GGGCATACCTTTATCCTGAG-3′, RV, 5′-CCACTGAAGTCATCCATGTC-3′; and β2M: FW, 5′-CACCCCACTGAGACTGATACA-3′, RV, 5′-TGATGCTTGATCACATGTCTCG-3′.

Microarray analysis and gene expression profiles

Total RNA was isolated using high pure RNA isolation kit (Roche). The yield of the extracted RNA was determined spectrophotometrically by measuring the OD at 260 nm. The purity and quality of extracted RNA were evaluated using the Experion RNA StdSens Analysis kit (Bio-Rad Laboratories). High-quality RNA with RNA Quality Indicator (RQI) score >8 was used for microarray experiments. Gene expression profiling was performed using Illumina's multisample format Mouse WG-6 V2 BeadChip that contains 45,281 transcripts and profiles 6 samples simultaneously on a single chip (Illumina). Raw microarray intensity data were analyzed with the Genome Studio software normalized using the quantile normalization method according to the manufacturer's recommendation. Differential analysis were performed for each group and the data were filtered on differential score >30 or less than −30, which is equivalent to $p < 0.001$. The probes were considered as expressed by filtering data on detection $p < 0.01$. Results of the microarray analysis are accessible on National Center for Biotechnology Information Gene Expression Omnibus (Gene Expression Omnibus accession number GSE66782; http://www.ncbi.nlm.nih.gov/geo/query/acc.cgi?acc=GSE66782).

Statistical analysis

Cytokine production, NO, and urea levels were compared between DUSP3$^{+/+}$ and DUSP3$^{-/-}$ cells using one-way ANOVA. Differences in survival were determined by Kaplan–Meier analysis. All tests were performed using GraphPad-Prism software (GraphPad Software). A p value < 0.05 was considered significant.

Results

DUSP3 is strongly expressed in monocytes and macrophages

A previous study analyzing the gene expression profile of protein phosphatases in different murine immune cell types showed that *Dusp3* is the most strongly expressed A-*DSP*–encoding gene in macrophages (22). We performed an analysis on the Genevestigator online platform and found that DUSP3 is expressed at high levels in macrophages (Fig. 1A). To confirm this finding, we quantified DUSP3 expression by Western blot in lysates from different mouse organs. Cells harvested from the peritoneal cavity had a higher expression level of this phosphatase than the other organs (Fig. 1B). Furthermore, we found that PMs express higher levels of DUSP3 than sorted T and B cells (Fig. 1C).

To investigate *DUSP3* expression level in human monocytes, we analyzed the gene expression profiles of populations of peripheral blood cells from 256 healthy volunteers. CD14$^+$ monocytes expressed a higher level of *DUSP3* mRNA than CD4$^+$ T cells, CD8$^+$ T cells, CD19$^+$ B cells, and CD15$^+$ neutrophils (Fig. 2A). We next analyzed the expression levels of all DSPs in human monocytes and found that *DUSP3* was strongly expressed among A-DSPs, as was the expression of the typical DSPs DUSP1/MKP1 and DUSP6/MKP3 (Fig. 2B). At the protein level, monocytes and monocyte-derived macrophages expressed greater levels of DUSP3 than neutrophils, B cells, and T cells (Fig. 2C).

DUSP3$^{-/-}$ mice are resistant to inflammatory shock induced by LPS or CLP

The strong expression of DUSP3 in monocytes and macrophages suggests that it plays an important role in inflammation and innate

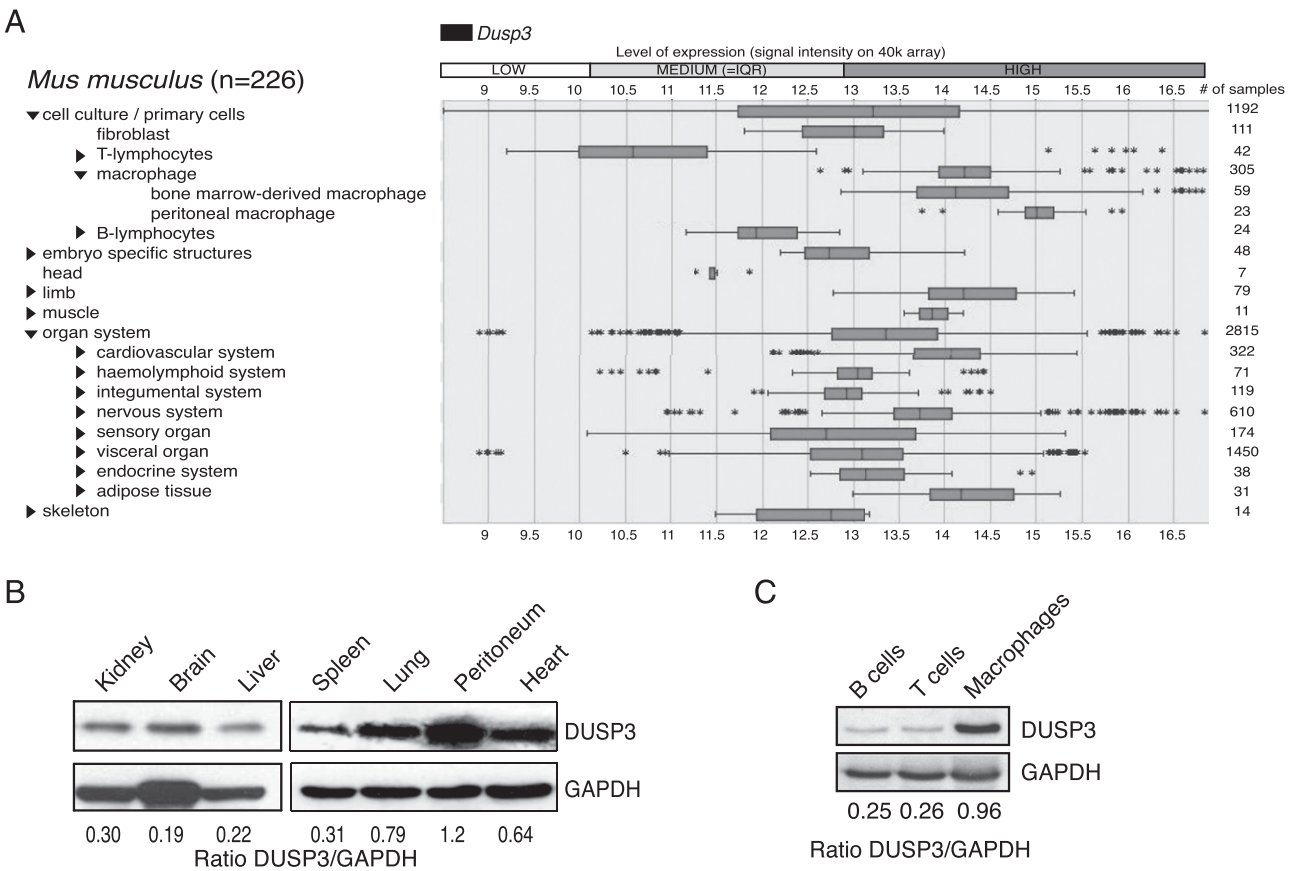

FIGURE 1. DUSP3 is strongly expressed in mouse macrophages. (**A**) *Dusp3* expression levels in different tissues and cell lines, extracted from the Genevestigator database (http://www.genevestigator.com). (**B**) Western blot analysis of DUSP3 protein expression in proteins extracts of mouse organs. (**C**) Western blot analysis of DUSP3 protein expression in sorted B lymphocytes, T lymphocytes, and macrophages from mouse peritoneal cavity.

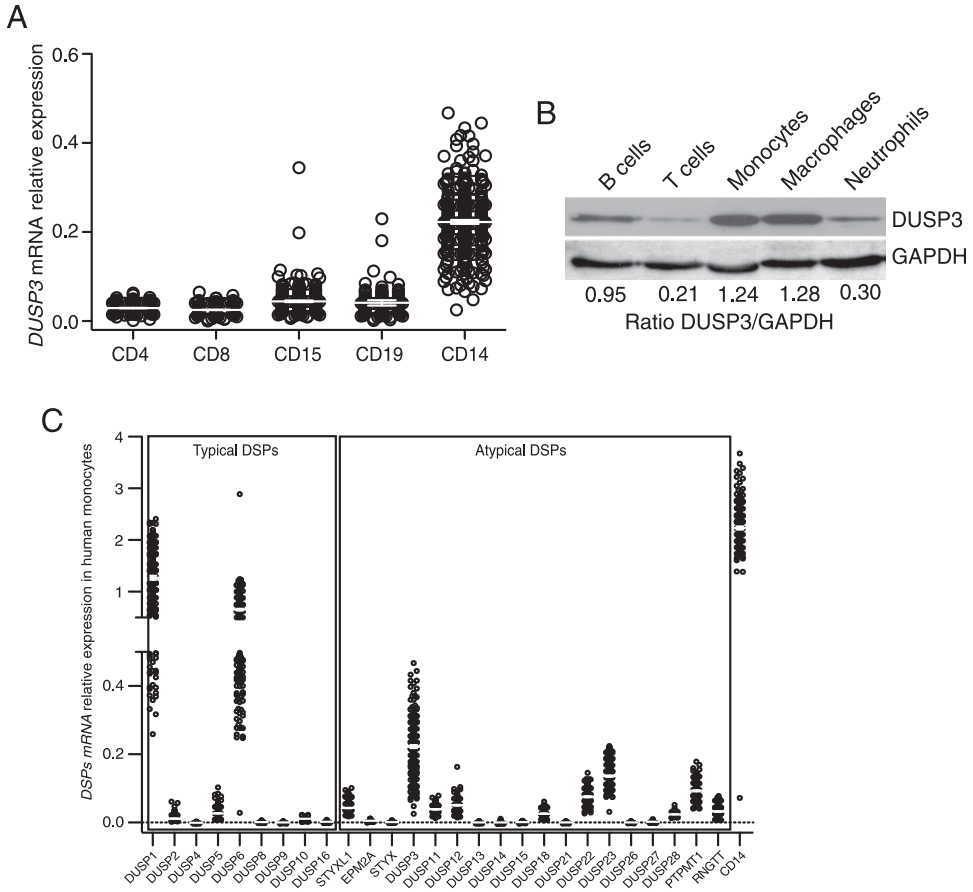

FIGURE 2. DUSP3 is strongly expressed in human monocytes and macrophages. (**A**) mRNA relative expression level of *DUSP3* gene in sorted human PBMC $CD4^+$T, $CD8^+$T, $CD19^+$B, neutrophils ($CD15^+$), and monocytes ($CD14^+$). (**B**) Microarray analysis of the expression of genes encoding A-typical and typical DSPs in human $CD14^+$ sorted monocytes. CD14 was used as a positive control for monocytes expressing mRNA. Data are presented as ratio of the fluorescence intensity for the DSP probe of interest and the mean fluorescence intensity for the housekeeping genes of each sample. A negative value corresponds to an expression below background level. Results are presented as mean ± SEM. (**C**) Western blot analysis of DUSP3 protein expression in sorted human B and T lymphocytes, neutrophils, monocytes, and monocyte-derived macrophages isolated from peripheral blood of healthy donors. GAPDH expression is shown as a loading control. Densitometric ratios of DUSP3 to GAPDH are shown for each representative Western blot.

immunity. At basal levels, we found that DUSP3 deletion does not significantly affect hematological parameters such as B and T lymphocytes, neutrophils, monocytes, and platelets counts (23). We examined the effect of in vivo LPS challenge in $DUSP3^{-/-}$ mice and their $DUSP3^{+/+}$ littermates. Mice were i.p. injected with a lethal dose of LPS, and survival was monitored for 7 d, after which no further deaths occurred. $DUSP3^{-/-}$ mice were fully resistant, whereas $DUSP3^{+/+}$ littermates were sensitive to LPS-induced endotoxic shock (Fig. 3A). Body temperature of $DUSP3^{-/-}$ mice decreased after LPS injection but remained significantly higher than in $DUSP3^{+/+}$ mice 6 h after LPS injection (Fig. 3B). Eighteen hours later, $DUSP3^{-/-}$ mice had recovered, whereas $DUSP3^{+/+}$ mice remained hypothermic (Fig. 3B).

Because the LPS injection model has a limited value to investigate TLR4-induced inflammatory responses, we used the more relevant polymicrobial sepsis model based on CLP and monitored the body temperature and survival of the mice. All mice received two doses of antibiotics (25 mg/kg ceftriaxone and 15 mg/kg metronidazole) 8 and 24 h after CLP. $DUSP3^{-/-}$ mice survived significantly better after CLP than $DUSP3^{+/+}$ mice. Indeed, at the end of the experiment (7 d), 70% of $DUSP3^{-/-}$ mice had survived compared with only 10% of $DUSP3^{+/+}$ mice (Fig. 3C). Both groups of mice were hypothermic 6 h after surgery, but 24 h after CLP, $DUSP3^{-/-}$ mice had recovered whereas $DUSP3^{+/+}$ mice had not recovered (Fig. 3D).

We next measured the systemic levels of IL-6 and TNF in plasma samples after LPS challenge and CLP. In the latter case, we also measured cytokine production in the peritoneal cavity. TNF production levels were significantly lower in $DUSP3^{-/-}$ mice than in $DUSP3^{+/+}$ mice at all the time points analyzed, after LPS challenge (Fig. 3E) and after CLP (Fig. 3F and 3G). IL-6 production was also significantly lower in the peritoneum of $DUSP3^{-/-}$ mice 6 h after CLP (Fig. 3J). Plasma IL-6 levels were also lower in $DUSP3^{-/-}$ mice, but the difference was not statistically significant (Fig. 3H and 3I).

To determine whether the defective TNF production in $DUSP3^{-/-}$ mice after LPS injection or CLP was due to an intrinsic defect in PMs, we collected these cells from mice, activated them ex vivo with LPS (1 μg/ml), and then measured TNF and IL-6 transcripts and proteins. DUSP3-deficient macrophages produced significantly less TNF and IL-6 after LPS stimulation (Fig. 4A and 4B). The lower level of TNF protein was due at least partially to reduced mRNA levels.

$DUSP3^{-/-}$ mice show signs of tolerance to shock after LPS and CLP

To investigate whether the observed resistance of $DUSP3^{-/-}$ mice to CLP-induced septic shock was associated with more efficient bacterial clearance, we compared bacterial counts in $DUSP3^{-/-}$ and $DUSP3^{+/+}$ mice after CLP. Six hours after surgery, the bacterial count was significantly lower in the peritoneal cavity of $DUSP3^{-/-}$ compared with $DUSP3^{+/+}$ mice (Fig. 5A). However, there was no difference 24 h after CLP. Bacterial counts in peripheral blood were equal in $DUSP3^{-/-}$ and $DUSP3^{+/+}$ mice 24 h after surgery (Fig. 5B). Because $DUSP3^{-/-}$ mice significantly survived CLP, our data suggest that they are tolerant to bacteria. This hypothesis was supported by the reduced systemic TNF and IL-6 production in $DUSP3^{-/-}$ mice after CLP (Fig. 3F, 3G, 3I, and 3J). Furthermore, the concentration of urea and NO, prominent macrophages products generated by arginase and inducible NO synthase, respectively, and both associated with tissue damage, remained at significantly lower levels in $DUSP3^{-/-}$ mice compared with $DUSP3^{+/+}$ mice, after CLP or LPS challenge (Fig. 5C and 5D).

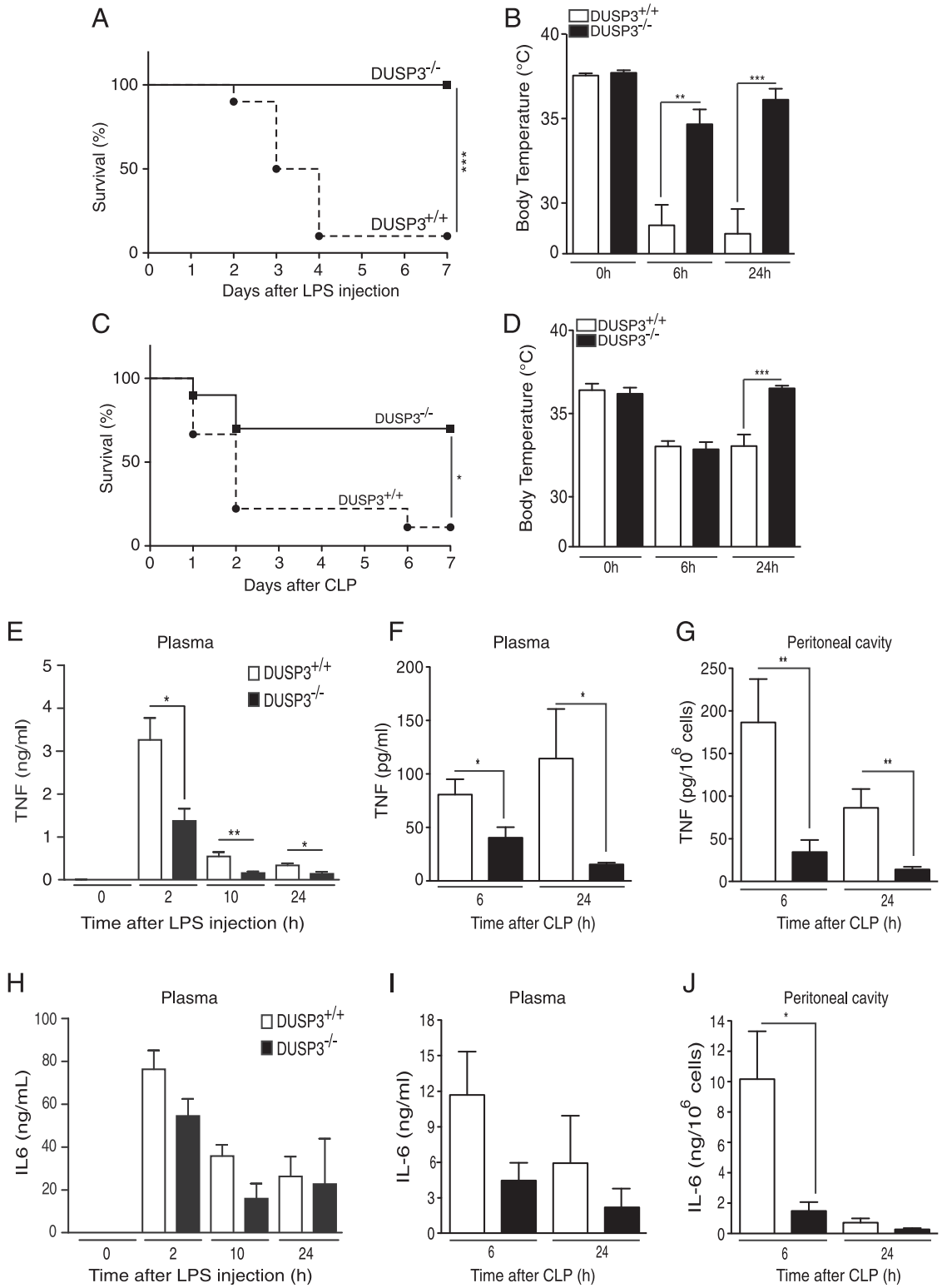

FIGURE 3. DUSP3$^{-/-}$ mice are resistant to LPS-induced endotoxemia and to CLP-induced septic shock. (**A**) DUSP3$^{+/+}$ (n = 17) and DUSP3$^{-/-}$ (n = 19) mice were injected i.p. with 6 mg/kg LPS. Percent survival was documented daily. (**B**) Body temperature of DUSP3$^{+/+}$ and DUSP3$^{-/-}$ mice before, 6 h, and 24 h after LPS injection. (**C**) DUSP3$^{+/+}$ (n = 20) and DUSP3$^{-/-}$ (n = 20) mice were subjected to CLP (one puncture with 21-gauge needle). Survival was documented daily for 7 d. Mortality incidence rates were compared using Kaplan–Meir with log-rank test performed by GraphPrism. (**D**) Body temperature of DUSP3$^{+/+}$ and DUSP3$^{-/-}$ mice before, 6 h, and 24 h after CLP. Results presented are a combination of two independent experiments. (**E**–**J**) CBA for IL-6 and TNF on serum samples from DUSP3$^{-/-}$ and DUSP3$^{+/+}$ mice at basal levels and 2, 10, and 24 h after i.p. injection of 6 mg/kg LPS (E and H), on serum and peritoneal cavity samples from DUSP3$^{-/-}$ and DUSP3$^{+/+}$ mice at 6 and 24 h after CLP (F and I), and on the peritoneal cavity cell-free liquid (G and J). Results are presented as mean ± SEM. n = 5 mice per group/time point. *$p < 0.05$, **$p < 0.01$, ***$p < 0.001$.

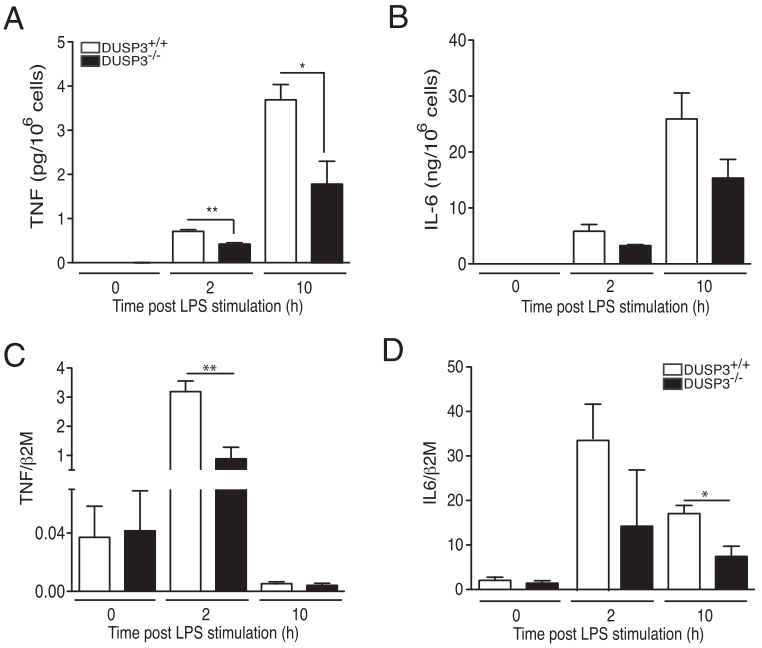

FIGURE 4. DUSP3$^{-/-}$ macrophages produce less TNF than DUSP3$^{+/+}$ in response to LPS. (**A** and **B**) DUSP3$^{+/+}$ and DUSP3$^{-/-}$ PMs were activated ex vivo with LPS (1 μg/ml). Cells supernatants were collected at 0, 2, and 10 h after activation. TNF (A) and IL-6 (B) concentration were determined using CBA. (**C** and **D**) IL-6 and TNF relative to β2M mRNA expression levels in PMs of DUSP3$^{+/+}$ and DUSP3$^{-/-}$ activated ex vivo with LPS (1 μg/ml) for 2 and 10 h. Results are presented as mean ± SEM. Three macrophage pools prepared from three mice each were analyzed separately. *$p < 0.05$, **$p < 0.01$.

In DUSP3$^{-/-}$ mice, resistance to LPS and CLP is associated with increased presence of M2-like alternatively activated macrophages

Because macrophages and neutrophils play important roles during microbial infection and in response to endotoxin, we quantified them in the peritoneum of DUSP3$^{+/+}$ and DUSP3$^{-/-}$ mice in basal conditions and after LPS challenge or CLP. The percentage of total macrophages, out of total live cells (Ly6G$^-$/CD11b$^+$/F4-80$^+$), was significantly higher in DUSP3$^{-/-}$ than in DUSP3$^{+/+}$ mice at basal levels (Fig. 6A). This difference remained significant after LPS challenge or CLP (Fig. 6A). However, the percentages of neutrophils (Fig. 6B) and myeloperoxidase production by activated neutrophils (data not shown) were similar in the two mouse groups in all the conditions analyzed.

Given the reduced proinflammatory response in DUSP3$^{-/-}$ mice and because this feature is characteristic of alternatively activated macrophages (M2/M2-like) (24), we hypothesized that DUSP3 deficiency could be associated with a dominance of M2-like anti-inflammatory macrophages. To investigate this hypothesis, we phenotyped DUSP3$^{-/-}$ and DUSP3$^{+/+}$ PMs based on the characterization described by Ghosn et al. (25). M1-like macrophages were F4/80^{int}CD11b^{int}Ly6G$^-$CD11c$^-$MHCII$^+$CCR2$^+$, whereas M2-like macrophages were F4/80^{hi}CD11b^{hi}Ly6G$^-$CD11c$^-$MHCII^{low}CCR2$^+$ (Fig. 6C and data not shown).

Under resting conditions, the percentage of M2-like macrophages (out of total macrophages) was significantly higher in the peritoneum of DUSP3$^{-/-}$ (55.68 ± 4.924%) than in DUSP3$^{+/+}$ mice (32.98 ± 3.31%), whereas no difference was observed for

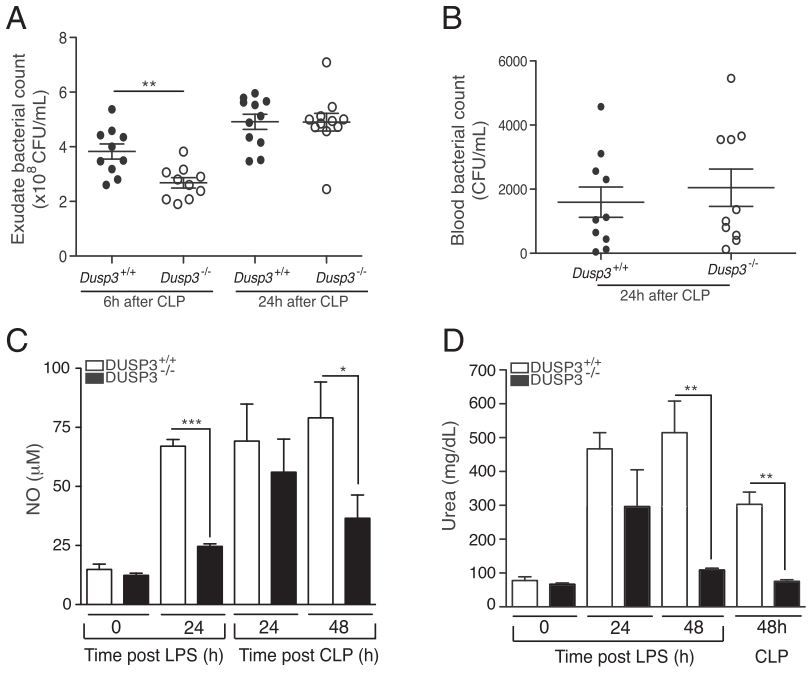

FIGURE 5. DUSP3 deficiency promotes tolerance to septic shock. (**A** and **B**) Bacterial colonies count in the peritoneum (A) and in the peripheral blood (B) of DUSP3$^{+/+}$ and DUSP3$^{-/-}$ mice at the indicated time points after CLP. All mice used for the 24-h time point received one dose of antibiotics (25 mg/kg ceftriaxone and 15 mg/kg metronidazole) 8 h after surgery. Each circle represents a single mouse. Open circles represent DUSP3$^{-/-}$, and dark circles represent DUSP3$^{+/+}$ mice. Horizontal lines represent mean ± SEM. (**C** and **D**) Plasma nitrate (C) and urea (D) levels of DUSP3$^{+/+}$ and DUSP3$^{-/-}$ mice at basal levels and at the indicated time points after CLP surgery or after LPS i.p. administration ($n = 5$ mice/group/time point). Results are presented as mean ± SEM. *$p < 0.05$, **$p < 0.001$, ***$p < 0.001$.

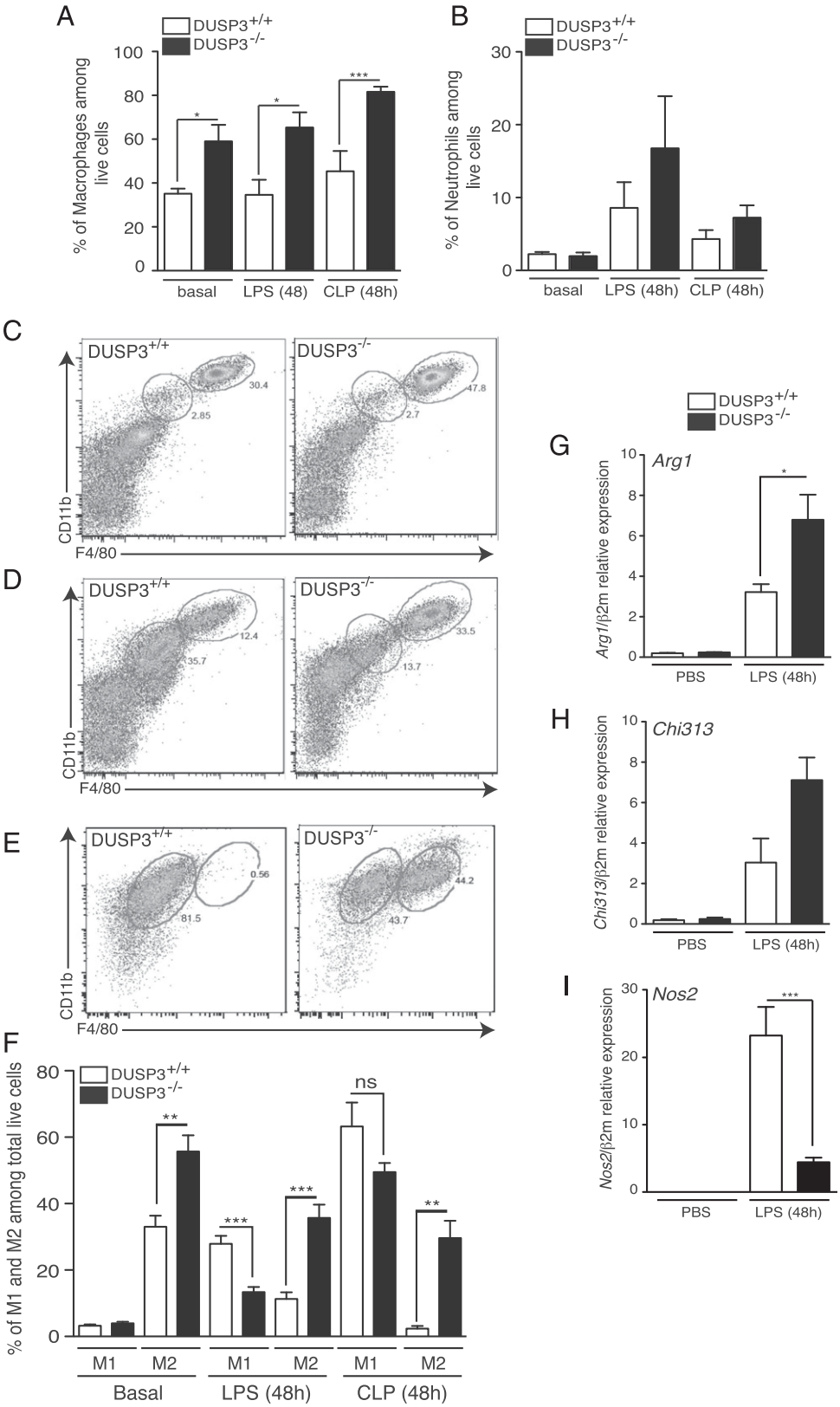

FIGURE 6. DUSP3 deficiency is associated with a dominance of M2-like over M1-like PMs. Peritoneal cells harvested from PBS-treated, LPS (6 mg/kg), or CLP-challenged DUSP3$^{-/-}$ (solid bars) and DUSP3$^{+/+}$ (open bars) mice and analyzed by flow cytometry for CD11b, F4/80, and Ly6G to discriminate between macrophages (Ly6G^{-}/CD11b^{+}/F4-80^{+}) and neutrophils (Ly6G^{+}/CD11b^{+}/F4/80^{-}). Percentage of macrophages (**A**) and neutrophils (**B**) out of total live cells are presented as histogram of means ± SEM. (**C**–**F**) Peritoneal cells from PBS-treated, LPS (6 mg/kg), or CLP-challenged DUSP3$^{-/-}$ and DUSP3$^{+/+}$ mice analyzed by flow cytometry to discriminate macrophages subtypes. F4/80^{high}CD11b^{high} (M2-like) and F4/80^{int}CD11b^{int} (M1-like) were gated out of total live cells extracted from PBS (C), 48-h LPS (6 mg/kg) challenged (D), or 48 h after CLP challenged (E) DUSP3$^{-/-}$ and DUSP3$^{+/+}$ mice. (F) Quantification of M1-like and M2-like cells extracted from PBS, LPS, or CLP-challenged mice. n = 6–10 mice in each group. PMs were extracted from DUSP3$^{+/+}$ and DUSP3$^{-/-}$ mice PBS- or LPS-treated for 48 h (6 mg/kg). Quantitative RT-PCR was performed to quantify the expression of *Arg1* (**G**), *Chi313* (**H**), and *Nos2* (**I**). The expression of gene of interest was relative to β2M. n = 3 mice in each experimental group. Results are presented as mean ± SEM. *$p < 0.05$, **$p < 0.01$, ***$p < 0.001$.

M1-like macrophages (Fig. 6C and 6F). Forty-eight hours after LPS injection, DUSP3$^{+/+}$ mice showed a highly significant increase of M1 macrophages and a significant decrease of M2 macrophages. However, the shift toward M1-like cells was less prominent in DUSP3$^{-/-}$ mice. M2-like macrophages remained the most dominant population in DUSP3$^{-/-}$ mice after LPS administration (Fig. 6D and 6E). Furthermore, in CLP-induced septic shock, there was a striking shift to the M1-like phenotype (61.2 ± 7.209%) and almost complete absence of M2-like cells (2.378 ± 0.7929%) in DUSP3$^{+/+}$ mice. In contrast, DUSP3$^{-/-}$ PMs were a mixture of both M1-like and M2-like cells, although M1-like macrophages were dominant (Fig. 6E and 6F). We also measured the expression of the genes associated with M1-like and M2-like PMs, namely, *Nos2*, *Arg1*, and *Chi313* (*Ym1*). After LPS challenge, *Arg1* (Fig. 6G) and *Chi313* (Fig. 6H) expression were increased in DUSP3$^{-/-}$ mice, whereas *Nos2* (Fig. 6I) was markedly increased in DUSP3$^{+/+}$ macrophages.

Monocytes and macrophages confer resistance to LPS-induced shock in DUSP3$^{-/-}$ mice

To investigate the role of DUSP3$^{-/-}$ myeloid cells in the observed phenotype, we generated chimeric mice by transplantation of BM from DUSP3$^{-/-}$-C57BL/6-CD45.2 mice into lethally irradiated WT-C57BL/6-CD45.1 mice (DUSP3$^{-/-}$ > WT). Successful hematolymphoid reconstitution was verified by flow cytometry 3 wk after transplantation (data not shown). The chimeric mice were challenged with LPS. As a control, irradiated WT-C57BL/6-CD45.1 mice were transplanted with DUSP3$^{+/+}$-C57BL/6-CD45.2 BM cells (WT > WT). Survival after LPS challenge was monitored for 8 d. Notably, >70% of DUSP3$^{-/-}$ > WT mice survived until the end of the experiment compared with only 9% of DUSP3$^{+/+}$ > WT mice (Fig. 7A). Body temperature decreased 24 h after LPS challenge in all mice, but then increased significantly to almost normal values in DUSP3$^{-/-}$ > WT mice (Fig. 7B). To investigate whether monocytes contributed to the resistance to LPS, we transferred DUSP3$^{-/-}$ BM sorted

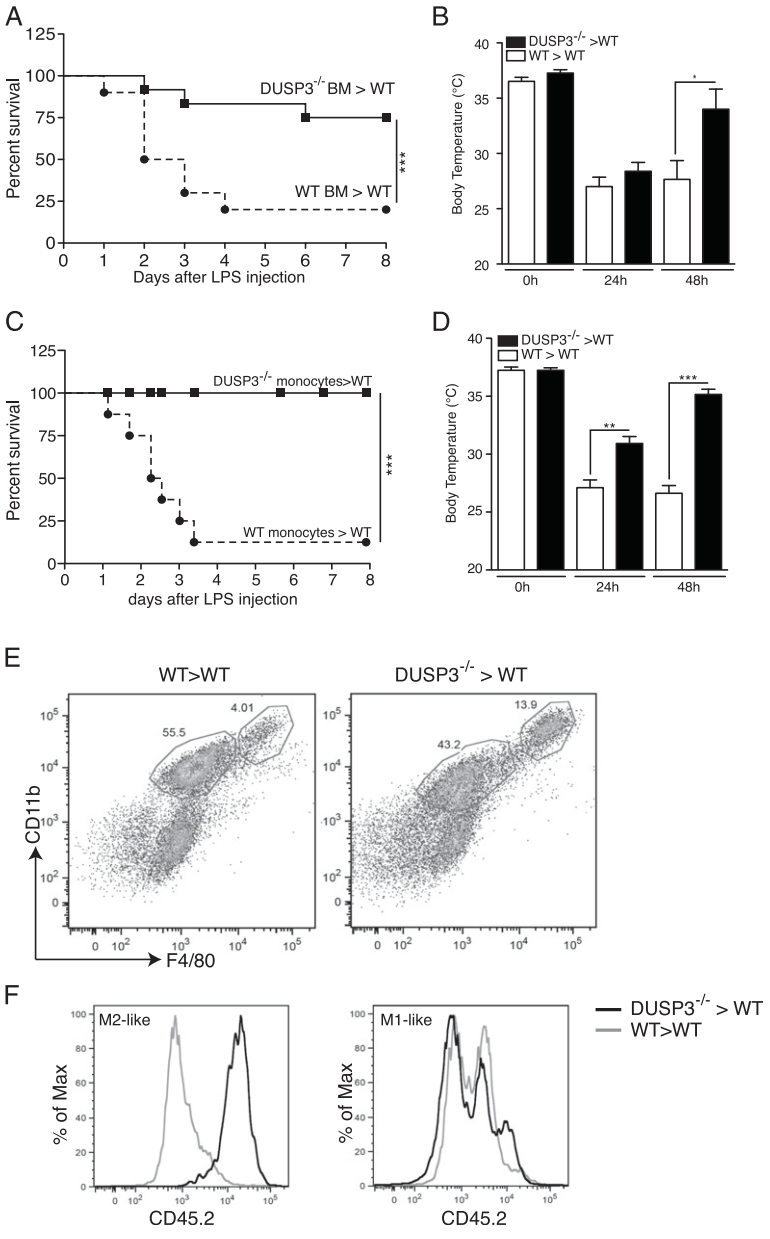

FIGURE 7. Adoptive transfer of DUSP3$^{-/-}$ BM or monocytes confers resistance of WT mice to LPS. (**A** and **B**) Percent survival to LPS challenge (A) and body temperature (B) of irradiated WT-CD45.1 mice transplanted with DUSP3$^{-/-}$-CD45.2 (DUSP3$^{-/-}$BM > WT) or DUSP3$^{+/+}$-CD45.2 (WT BM > WT)–derived BM cells. (**C** and **D**) Percent survival to LPS challenge (6 mg/ml) (C) and body temperature (D) of WT-CD45.1 mice transplanted with monocytes (1.5 × 10^6) from DUSP3$^{-/-}$-CD45.2 (DUSP3$^{-/-}$>WT) or DUSP3$^{+/+}$-CD45.2 (WT > WT) mice. Incident of lethality were compared and analyzed using Kaplan–Meir with log-rank test performed by GraphPrism. n = 6 mice in each experimental group. (**E**) Representative FACS dot plots showing the staining for CD11b and F4/80 gated on live singlets peritoneal cavity cells 48 h after LPS (6 mg/kg) challenge of WT > WT and DUSP3$^{-/-}$ > WT. (**F**) CD45.2 surface expression on gated M1-like and M2-like cells shown in (E). Results are shown as percent of maximum (% of Max) of overlaid histograms of the gated populations shown in (E).

monocytes (1.5×10^6 cells) to WT-(C57BL/6-CD45.1) mice ($DUSP3^{-/-} >$ WT). As a control, $DUSP3^{+/+}$ BM sorted monocytes were transferred to WT (C57BL/6-CD45.1) mice (WT > WT). After 24 h, recipient mice were i.p. challenged with LPS, and survival and body temperature were monitored. As shown in Fig. 7C, transfer of $DUSP3^{-/-}$ monocytes to WT mice conferred full resistance to LPS. Variations of body temperatures of mice were compatible with survival outcome (Fig. 7D). Interestingly, the resistance of $DUSP3^{-/-} >$ WT mice to LPS was associated with increased presence of donor-derived ($CD45.2^+$) M2-like macrophages ($F4/80^{hi}CD11b^{hi}$) in the peritoneal cavity of recipient mice (Fig. 7E and 7F). However, M1-like macrophages ($F4/80^{int}CD11b^{int}$) were a mixture of CD45.1 (recipient) and CD45.2 (donor) (Fig. 7E and 7F).

DUSP3 deficiency affects ERK1/2 activation but not JNK, p38, or NF-κB pathways after TLR4 triggering

Several DSPs have been reported as early responsive genes induced upon LPS stimulation. The most documented is probably DUSP1/MKP1 (26). Therefore, we wanted to investigate whether DUSP3 expression is also regulated after TLR4 stimulation. We compared DUSP3 expression at basal levels and at 1.5–2 and 24 h after ex vivo activation of $DUSP3^{+/+}$ PMs with LPS (1 μg/ml). In contrast with other LPS-induced DSPs, DUSP3 expression is not induced after TLR4 activation (Fig. 8A and 8B). To investigate whether the observed phenotype is due to a simple redundancy of another DSP in the absence of DUSP3 in vivo, we performed a microarray analysis to evaluate the expression levels of all DSPs transcripts in the PMs retrieved from $DUSP3^{-/-}$ and $DUSP3^{+/+}$ mice 36 h after LPS or PB injection. We found that *Dusp3* deletion does not affect the expression of the other DSPs, both typical and atypical. Furthermore, and in a DUSP3 expression–independent manner, we found that LPS challenge increased significantly the expression of the MKP transcripts *Dusp1* (MKP1), *Dusp2* (MKP2), and *Dusp16* (MKP7), and decreased significantly the expression of the A-DSP transcript *Epm2a* (Laforin) (Fig. 8C and 8D).

One of the major inflammatory signaling pathways activated after TLR4 triggering is the NF-κB pathway (5). To investigate whether DUSP3 deficiency is associated with a defect in this signaling pathway, we evaluated the expression level of IκBα (which is degraded to allow NF-κB activation) before and at several time points after stimulation of PMs with LPS (1 μg/ml).

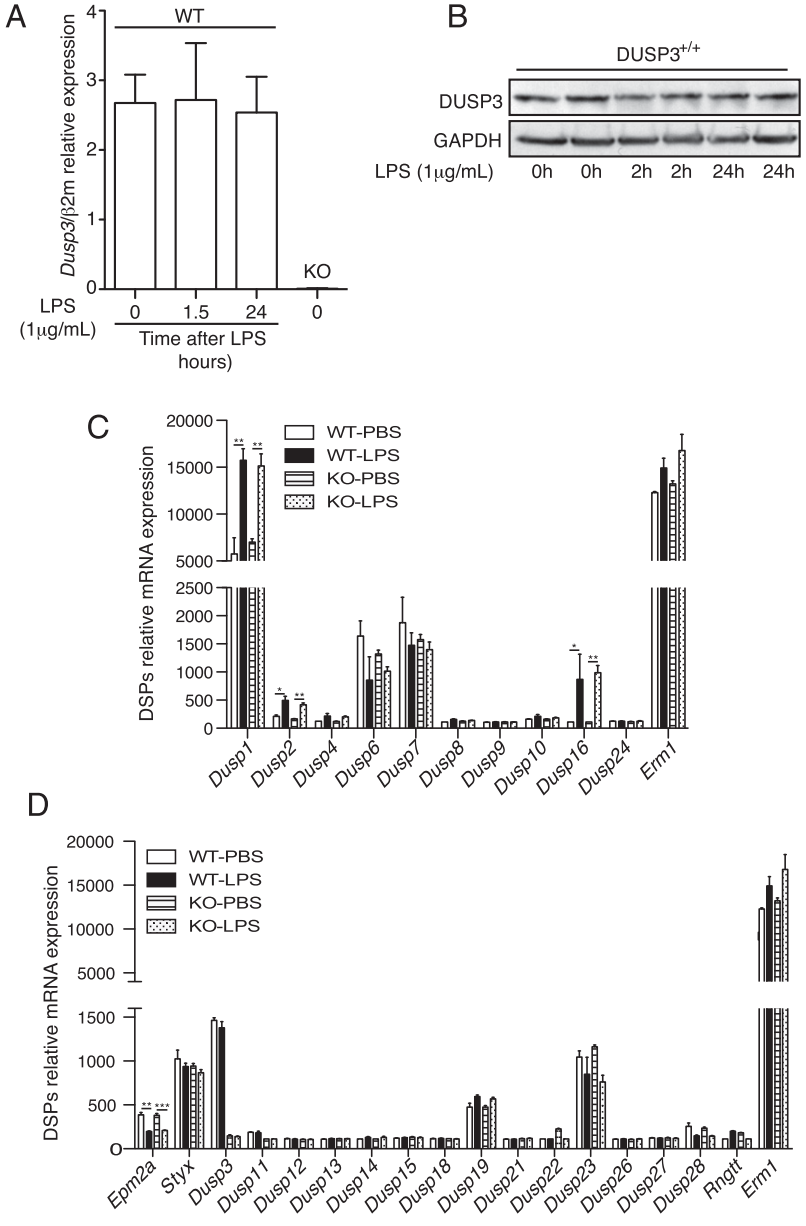

FIGURE 8. DUSP3 deletion does not affect other DSPs expression. (**A** and **B**) PMs isolated from 10- to 12-wk-old $DUSP3^{+/+}$ and $DUSP3^{-/-}$ mice were stimulated ex vivo with 1 μg/ml LPS for the indicated time points. (A) Quantitative RT-PCR was performed to quantify the expression of *Dusp3* gene. The expression was relative to β2M. $n = 3$ mice in each experimental group. (**C** and **D**) Total RNA was isolated from PMs of $DUSP3^{+/+}$ and $DUSP3^{-/-}$ 36 h after PBS or LPS (6 mg/kg) injection. Gene expression profiling was performed using Illumina's multisample format Mouse WG-6 V2 BeadChip. The expression of all typical DSPs (MKPs) (C) and atypical (D) are shown. Erm1 (F4/80) was used as a positive control for macrophages expressing mRNA. Data are presented as mean ± SEM of the fluorescence intensity for the DSP probe of interest. $n = 3$ mice in each group. $^*p < 0.05$, $^{**}p < 0.01$, $^{***}p < 0.001$ determined using unpaired t test.

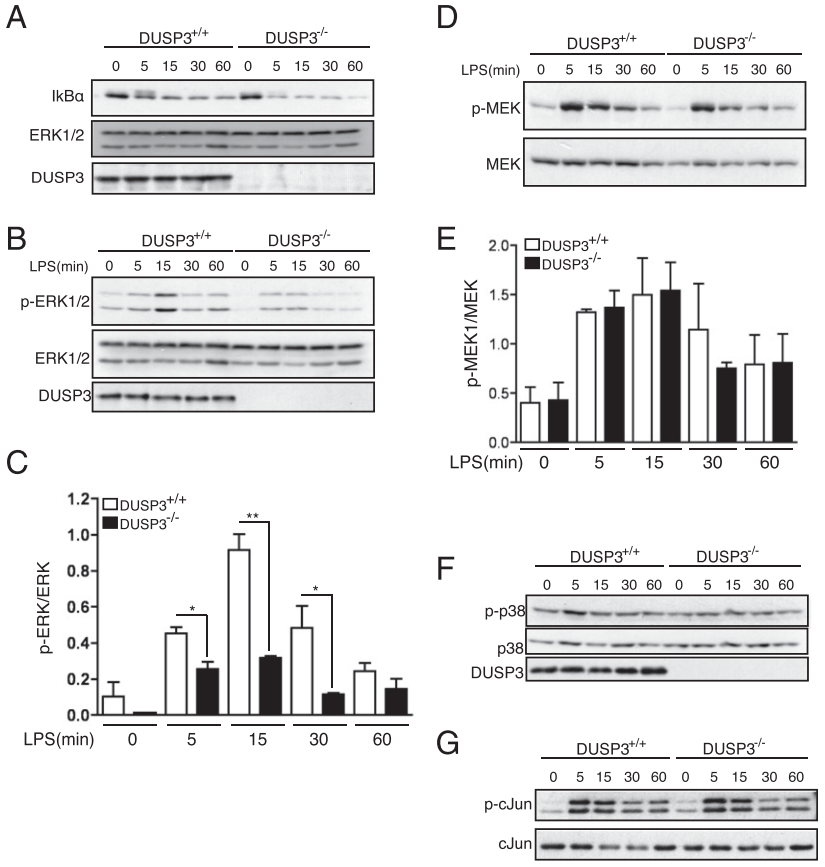

FIGURE 9. DUSP3 deficiency affects ERK1/2 phosphorylation, but not JNK, p38, or NF-κB pathways after TLR4 triggering. PMs isolated from 10- to 12-wk-old DUSP3$^{+/+}$ and DUSP3$^{-/-}$ mice were stimulated ex vivo with 1 μg/ml LPS for the indicated time points. Equal amount of proteins were loaded on SDS-PAGE, and Western blots were performed using (**A**) anti-IκB Ab and anti-ERK1/2 as a loading control, (**B**) anti–phospho-ERK1/2 (Thr^{202}/Tyr^{204}) and anti-ERK1/2 as a loading control, (**D**) anti–phospho-MEK1/2 (Ser$^{217/221}$) and anti-MEK1/2, and anti–phospho-p38 (Thr^{180}/Tyr^{182}), and (**F**) anti-p38. (**C** and **E**) Densitometry quantification of phospho-ERK1/2/ERK1/2 (C) and phospho-MEK/MEK (E) were performed using ImageJ software. Results are presented as a ratio of phospho-ERK/ERK and phospho-MEK/MEK from three independent experiments. Data are shown as mean ± SEM. *$p < 0.05$, **$p < 0.01$, determined using unpaired t test. (**G**) JNK activity assay. Phospho-SAPK/JNK (Thr^{183}/Tyr^{185}) was immunoprecipitated from nonactivated and LPS-activated PM lysates. Recombinant c-Jun was used as a substrate for the kinase assay. JNK activity was revealed using anti–phospho–c-Jun (Ser^{63}). Representative JNK assay is shown.

As shown in Fig. 9A, TLR4 activation induced a rapid IκBα degradation in both DUSP3$^{-/-}$ and DUSP3$^{+/+}$ mice (Fig. 9A). These results suggest that NF-κB activation, in response to LPS, is not affected by DUSP3 deletion.

Earlier studies indicated that DUSP3 dephosphorylates ERK1/2 and JNK2, but not p38 (16). In addition, TLR4 activation leads to the activation of MAPK signaling pathways (27, 28). Therefore, we investigated whether the activation of these MAPKs was affected by DUSP3 deficiency in PMs. We probed ERK1/2 with phospho-specific Abs at basal levels and after stimulation of DUSP3$^{+/+}$ and DUSP3$^{-/-}$ PMs with 1 μg/ml LPS. Surprisingly, and in contradiction with all in vitro studies published to date, DUSP3 deficiency in vivo was not associated with increased ERK1/2 phosphorylation. Indeed, the basal phosphorylation level of ERK1/2 in the DUSP3$^{-/-}$ PMs was lower than in DUSP3$^{+/+}$ PMs. After LPS treatment, ERK1/2 phosphorylation increased slightly in DUSP3$^{-/-}$ PMs but remained significantly lower than in DUSP3$^{+/+}$ PMs (Fig. 9B and 9C). We next checked for the activation of the ERK1/2 upstream MAPK, MAPKK1/2, or MEK1/2 phosphorylation status (29). Western blot analysis using anti–phospho-MEK1/2 Ab showed that MEK1/2 activation was not altered in DUSP3-deficient PMs either at the basal level or after ex vivo LPS activation (Fig. 9D and 9E). DUSP3 deficiency did not affect p38 and JNK1/2 activation either (Fig. 9F and 9G).

Discussion

We report that DUSP3 is strongly expressed in monocytes and macrophages, and plays a critical role as a positive regulator of the innate immune response. We show that genetic deletion of DUSP3 confers strong protection against endotoxin shock and polymicrobial septic shock. This protection is associated with decreased systemic production of the proinflammatory cytokine TNF and dominance of M2-like macrophages. Interestingly, transfer of DUSP3$^{-/-}$ BM or monocytes to WT mice appears sufficient to transfer LPS resistance to the recipients. In the recipient mice, inflammatory responses associated with DUSP3 knockout are dominant over the WT response, as demonstrated by the dominance of CD45.2-DUSP3$^{-/-}$ M2-like macrophages over the recipient CD45.1-WT macrophages.

These findings suggest that the anti-inflammatory responses observed in DUSP3-deficient mice are, at least partially, due to suppression of cytokine production by macrophages and demonstrate an essential role for DUSP3 in regulating macrophage polarization and inflammation.

The bacterial load in the blood of DUSP3-deficient mice subjected to CLP did not differ from that in WT mice, yet DUSP3$^{-/-}$ mice resisted CLP, suggesting that DUSP3 deficiency confers disease tolerance without affecting the pathogen load. We also found that DUSP3 deficiency protected mice from lethal shock in the absence of bacteria, that is, when LPS challenge was used. In both cases (LPS and CLP), survival of the DUSP3$^{-/-}$ mice was associated with a lower level of systemic NO and urea, markers of tissue damage, in addition to a lower level of inflammatory mediators, such as TNF and IL-6, compared with controls. Tolerance to disease as a defense strategy was demonstrated decades ago in plants (30) and more recently in flies and in different mouse models of infection (31), including polymicrobial infection in severe sepsis (32, 33). However, the mechanisms of disease tolerance are poorly understood. In our model, tolerance to LPS and to CLP was associated with dominance of M2-like macrophages in the peritoneal cavity of DUSP3$^{-/-}$ mice. These macrophages were almost absent in DUSP3$^{+/+}$ mice after LPS or CLP challenge. In addition, we demonstrated that DUSP3-dependent resistance to shock was transferable via monocytes to WT mice and was associated with dominance of M2-like macrophages in the

peritoneal cavity of recipient mice. These data clearly suggest that the tolerance to disease caused by DUSP3 deficiency is mediated by M2-like macrophages. The role of these macrophages in sepsis and septic shock is not well understood. However, it has been reported that tolerance and M2 alternative macrophage polarization are related processes regulated by NF-κB p50 (34), and most probably also by other unknown molecular mechanisms. In addition, a mixed M1/M2 population has been observed in baboons surviving experimental peritonitis, whereas baboons that died had an exclusive M1 signature (35).

In contrast with DUSP1, DUSP3 expression is not regulated after TLR4 triggering. However, DUSP3 deletion does not affect the expression of any other member of DSPs group excluding a redundant effect on another DSP in the observed phenotype.

DUSP3 depletion does not affect TLR4/CD14 expression (data not shown) and IκB degradation, and thus does not affect NF-κB signaling either. This indicates that TLR4 signaling molecules such as MyD88, IRAK1-4, TRAF6, and TAK1 are not altered by DUSP3 deficiency because IκB degradation requires their activation after TLR4 stimulation (4).

In contradiction with previous findings (12–15), DUSP3 deletion was associated with decreased activity of ERK1/2 in PMs, whereas JNK1/2 and p38 activities were not affected. This was observed only in macrophages. Indeed, ERK1/2 and JNK1/2 activation in B cells, T cells, and platelets in response to BCR, TCR, and GPVI ligands were not affected by DUSP3 deletion (23). We cannot exclude the possibility that other phosphatases might compensate for the absence of DUSP3 in these cells in vivo.

Several studies, including ours, reported that ERK1/2 and JNK1/2, but not p38, were targeted by DUSP3 in different in vitro cellular models (12–15). However, ours is the first report, to our knowledge, on the physiological role of DUSP3 in macrophages and the consequences of its deletion on the activation of MAPKs.

The decrease in ERK1/2 activation in DUSP3-deficient macrophages is compatible with the decreased TNF production (transcript and protein) in both CLP and LPS models. Because the NF-κB activation pathway is not affected by DUSP3 deficiency, hypophosphorylation of ERK1/2 could explain the low TNF production in these cells. In line with this, a previous report showed that blocking ERK1/2 activation by pharmacological inhibitors was sufficient to substantially reduce TNF secretion (36). In this sense, by indirectly activating ERK1/2, DUSP3 controls the window of synthesis of proinflammatory cytokines such as TNF.

In conclusion, to our knowledge, our results are the first demonstration that DUSP3 plays a nonredundant role in the innate immune response. DUSP3 controls macrophage polarization by regulating TNF production and ERK activity not only in a sterile inflammation model, but also in a polymicrobial model of sepsis. DUSP3 deficiency protected mice from sepsis and septic shock induced by bacterial products by mechanisms involving M2-like macrophages. This finding suggests that regulation of the immune response by DUSP3 is more complex than a simple downregulation of proinflammatory cytokine production.

Acknowledgments

We are grateful to the GIGA-Animal, GIGA-Imaging, and GIGA-Geno-Transcriptomics Core Facilities for excellent technical assistance and support and Dr. Amin Bredan for editing the manuscript.

Disclosures

The authors have no financial conflicts of interest.

References

1. López-Bojórquez, L. N., A. Z. Dehesa, and G. Reyes-Terán. 2004. Molecular mechanisms involved in the pathogenesis of septic shock. *Arch. Med. Res.* 35: 465–479.
2. Cohen, J. 2002. The immunopathogenesis of sepsis. *Nature* 420: 885–891.
3. Rittirsch, D., M. A. Flierl, and P. A. Ward. 2008. Harmful molecular mechanisms in sepsis. *Nat. Rev. Immunol.* 8: 776–787.
4. Akira, S., and K. Takeda. 2004. Toll-like receptor signalling. *Nat. Rev. Immunol.* 4: 499–511.
5. Kawai, T., and S. Akira. 2010. The role of pattern-recognition receptors in innate immunity: update on Toll-like receptors. *Nat. Immunol.* 11: 373–384.
6. Kyriakis, J. M., and J. Avruch. 2012. Mammalian MAPK signal transduction pathways activated by stress and inflammation: a 10-year update. *Physiol. Rev.* 92: 689–737.
7. Alonso, A., J. Sasin, N. Bottini, I. Friedberg, I. Friedberg, A. Osterman, A. Godzik, T. Hunter, J. Dixon, and T. Mustelin. 2004. Protein tyrosine phosphatases in the human genome. *Cell* 117: 699–711.
8. Tautz, L., D. A. Critton, and S. Grotegut. 2013. Protein tyrosine phosphatases: structure, function, and implication in human disease. *Methods Mol. Biol.* 1053: 179–221.
9. Liu, Y., E. G. Shepherd, and L. D. Nelin. 2007. MAPK phosphatases—regulating the immune response. *Nat. Rev. Immunol.* 7: 202–212.
10. Jeffrey, K. L., M. Camps, C. Rommel, and C. R. Mackay. 2007. Targeting dual-specificity phosphatases: manipulating MAP kinase signalling and immune responses. *Nat. Rev. Drug Discov.* 6: 391–403.
11. Salojin, K., and T. Oravecz. 2007. Regulation of innate immunity by MAPK dual-specificity phosphatases: knockout models reveal new tricks of old genes. *J. Leukoc. Biol.* 81: 860–869.
12. Ishibashi, T., D. P. Bottaro, A. Chan, T. Miki, and S. A. Aaronson. 1992. Expression cloning of a human dual-specificity phosphatase. *Proc. Natl. Acad. Sci. USA* 89: 12170–12174.
13. Yuvaniyama, J., J. M. Denu, J. E. Dixon, and M. A. Saper. 1996. Crystal structure of the dual specificity protein phosphatase VHR. *Science* 272: 1328–1331.
14. Alonso, A., M. Saxena, S. Williams, and T. Mustelin. 2001. Inhibitory role for dual specificity phosphatase VHR in T cell antigen receptor and CD28-induced Erk and Jnk activation. *J. Biol. Chem.* 276: 4766–4771.
15. Rahmouni, S., F. Cerignoli, A. Alonso, T. Tsutji, R. Henkens, C. Zhu, C. Louis-dit-Sully, M. Moutschen, W. Jiang, and T. Mustelin. 2006. Loss of the VHR dual-specific phosphatase causes cell-cycle arrest and senescence. *Nat. Cell Biol.* 8: 524–531.
16. Cerignoli, F., S. Rahmouni, Z. Ronai, and T. Mustelin. 2006. Regulation of MAP kinases by the VHR dual-specific phosphatase: implications for cell growth and differentiation. *Cell Cycle* 5: 2210–2215.
17. Arnoldussen, Y. J., P. I. Lorenzo, M. E. Pretorius, H. Waehre, B. Risberg, G. M. Maelandsmo, H. E. Danielsen, and F. Saatcioglu. 2008. The mitogen-activated protein kinase phosphatase vaccinia H1-related protein inhibits apoptosis in prostate cancer cells and is overexpressed in prostate cancer. *Cancer Res.* 68: 9255–9264.
18. Henkens, R., P. Delvenne, M. Arafa, M. Moutschen, M. Zeddou, L. Tautz, J. Boniver, T. Mustelin, and S. Rahmouni. 2008. Cervix carcinoma is associated with an up-regulation and nuclear localization of the dual-specificity protein phosphatase VHR. *BMC Cancer* 8: 147.
19. Hao, L., and W. M. ElShamy. 2007. BRCA1-IRIS activates cyclin D1 expression in breast cancer cells by downregulating the JNK phosphatase DUSP3/VHR. *Int. J. Cancer* 121: 39–46.
20. Amand, M., C. Erpicum, K. Bajou, F. Cerignoli, S. Blacher, M. Martin, F. Dequiedt, P. Drion, P. Singh, T. Zurashvili, et al. 2014. DUSP3/VHR is a pro-angiogenic atypical dual-specificity phosphatase. *Mol. Cancer* 13: 108.
21. Rittirsch, D., M. S. Huber-Lang, M. A. Flierl, and P. A. Ward. 2009. Immunodesign of experimental sepsis by cecal ligation and puncture. *Nat. Protoc.* 4: 31–36.
22. Arimura, Y., and J. Yagi. 2010. Comprehensive expression profiles of genes for protein tyrosine phosphatases in immune cells. *Sci. Signal.* 3: rs1.
23. Musumeci, L., M. J. Kuijpers, K. Gilio, A. Hego, E. Théâtre, L. Maurissen, M. Vandereyken, C. V. Diogo, C. Lecut, et al. 2015. Dual-specificity phosphatase 3 deficiency or inhibition limits platelet activation and arterial thrombosis. *Circulation.* 131: 656–68.
24. Biswas, S. K., and A. Mantovani. 2010. Macrophage plasticity and interaction with lymphocyte subsets: cancer as a paradigm. *Nat. Immunol.* 11: 889–896.
25. Ghosn, E. E., A. A. Cassado, G. R. Govoni, T. Fukuhara, Y. Yang, D. M. Monack, K. R. Bortoluci, S. R. Almeida, L. A. Herzenberg, and L. A. Herzenberg. 2010. Two physically, functionally, and developmentally distinct peritoneal macrophage subsets. *Proc. Natl. Acad. Sci. USA* 107: 2568–2573.
26. Patterson, K. I., T. Brummer, P. M. O'Brien, and R. J. Daly. 2009. Dual-specificity phosphatases: critical regulators with diverse cellular targets. *Biochem. J.* 418: 475–489.
27. Takeda, K., and S. Akira. 2004. TLR signaling pathways. *Semin. Immunol.* 16: 3–9.
28. Yamamoto, M., and K. Takeda. 2010. Current views of toll-like receptor signaling pathways. *Gastroenterol. Res. Pract.* 2010: 240365.
29. Symons, A., S. Beinke, and S. C. Ley. 2006. MAP kinase kinase kinases and innate immunity. *Trends Immunol.* 27: 40–48.
30. Schafer, J. F. 1971. Tolerance to plant disease. *Annu. Rev. Phytopathol.* 9: 235–252.
31. Schneider, D. S., and J. S. Ayres. 2008. Two ways to survive infection: what resistance and tolerance can teach us about treating infectious diseases. *Nat. Rev. Immunol.* 8: 889–895.

32. Larsen, R., R. Gozzelino, V. Jeney, L. Tokaji, F. A. Bozza, A. M. Japiassú, D. Bonaparte, M. M. Cavalcante, A. Chora, A. Ferreira, et al. 2010. A central role for free heme in the pathogenesis of severe sepsis. *Sci. Transl. Med.* 2: 51ra71.
33. Figueiredo, N., A. Chora, H. Raquel, N. Pejanovic, P. Pereira, B. Hartleben, A. Neves-Costa, C. Moita, D. Pedroso, A. Pinto, et al. 2013. Anthracyclines induce DNA damage response-mediated protection against severe sepsis. *Immunity* 39: 874–884.
34. Porta, C., M. Rimoldi, G. Raes, L. Brys, P. Ghezzi, D. Di Liberto, F. Dieli, S. Ghisletti, G. Natoli, P. De Baetselier, et al. 2009. Tolerance and M2 (alternative) macrophage polarization are related processes orchestrated by p50 nuclear factor kappaB. *Proc. Natl. Acad. Sci. USA* 106: 14978–14983.
35. Mehta, A., R. Brewington, M. Chatterji, M. Zoubine, G. T. Kinasewitz, G. T. Peer, A. C. Chang, F. B. Taylor, Jr., and A. Shnyra. 2004. Infection-induced modulation of m1 and m2 phenotypes in circulating monocytes: role in immune monitoring and early prognosis of sepsis. *Shock* 22: 423–430.
36. Dumitru, C. D., J. D. Ceci, C. Tsatsanis, D. Kontoyiannis, K. Stamatakis, J. H. Lin, C. Patriotis, N. A. Jenkins, N. G. Copeland, G. Kollias, and P. N. Tsichlis. 2000. TNF-alpha induction by LPS is regulated posttranscriptionally via a Tpl2/ERK-dependent pathway. *Cell* 103: 1071–1083.